25

High-frequency Millimeter Wave Absorber Composed of a New Series of Iron Oxide Nanomagnets

Asuka Namai and Shin-ichi Ohkoshi
Department of Chemistry, School of Science, the University of Tokyo, Japan

1. Introduction

High-speed wireless communications using millimeter waves (30–300 GHz) have received much attention as a next-generation communication system capable of transmitting vast quantities of data such as high-definition video images. Due to the recent development of transistors composed of complementary metal-oxide semiconductors or double heterojunction bipolar transistors,[1-5] electromagnetic (EM) waves in the millimeter wave range are beginning to be used in high-speed wireless communication.[6-8] Especially, for 60 GHz-band wireless communication, Wigig alliance was established in December 2009, and televisions and local area network (LAN) using 60 GHz millimeter wave have been extensively researched and developed. Millimeter wave wireless communication is anticipated to realize a transmission rate that is several handred times greater than current wireless communication. On the other hand, in a wireless communication, electromagnetic interference (EMI) is a problem. In addition, the unnecessary EM waves should be eliminated to protect the human body, although the potential health effects due to the millimeter wave have not yet been understood.[9] To solve these problems, millimeter wave absorbers need to be equipped with electronic devices such as isolators or be painted on a wall of building, etc. However, currently materials that effectively restrain EMI in the region of millimeter waves almost do not exist. Thus, finding a suitable material has received much attention. Insulating magnetic materials absorb EM waves owing to natural resonance. Particularly, a magnetic material with a large coercive field (H_c) is expected to show a high-frequency resonance. In recent years, we firstly succeeded to obtain a single phase of ε-Fe_2O_3 nanomagnet (Figure 1), and found that ε-Fe_2O_3 nanomagnet exhibited an extremely large H_c value of 20 kOe at room temperature, which is the highest H_c value for insulating magnetic materials.[10-19] In this paper, we report a new millimeter wave absorber composed of ε-$Ga_xFe_{2-x}O_3$ ($0.10 \leq x \leq 0.67$) nanomagnets, which shows a natural resonance in the range of 35–147 GHz at room temperature.[20] This is the first example of a magnetic material which shows a natural resonance above 80 GHz. In addition, the study of the magnetic permeability of ε-$Ga_xFe_{2-x}O_3$ was performed in 60 GHz region (V-band). By analyzing electromagnetic wave absorption properties, the magnetic permeability (μ'-$j\mu''$) and dielectric constant (ε'-$j\varepsilon''$) of ε-$Ga_xFe_{2-x}O_3$ were evaluated.[21]

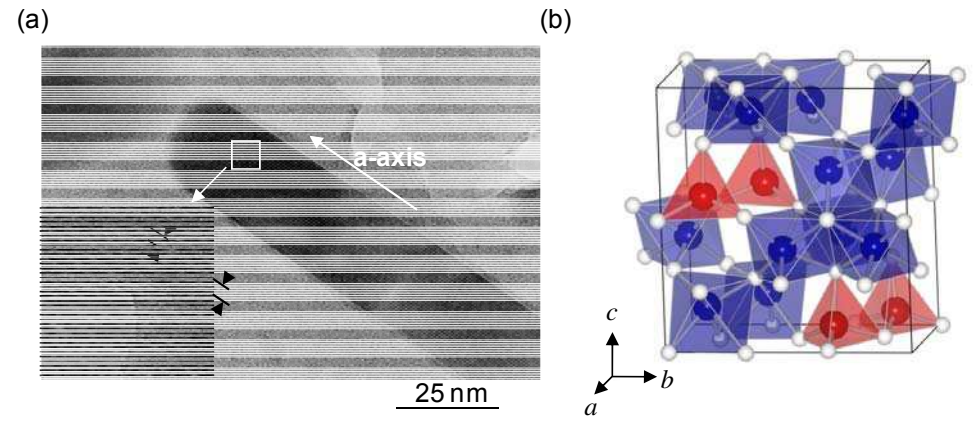

Fig. 1. (a) TEM image of ε-Fe_2O_3 at high magnification. The inset is the high resolution image. (b) Crystal structure of ε-Fe_2O_3.

2. Synthesis, crystal structures and magnetic properties

In this section, we show the synthesis, crystal structures and magnetic properties of a new millimeter-wave absorber composed of ε-$Ga_xFe_{2-x}O_3$ ($0.10 \leq x \leq 0.67$) nanoparticles.

2.1 Synthesis of ε-$Ga_xFe_{2-x}O_3$ nanomagnets

A new series of ε-$Ga_xFe_{2-x}O_3$ ($0.10 \leq x \leq 0.67$) nanoparticles was synthesized by the combination of reverse micelle and sol–gel techniques or only the sol–gel method. Figure 2 describes the flowchart of the synthetic procedure for ε-$Ga_xFe_{2-x}O_3$ nanoparticles. In the combination method between the reverse-micelle and sol-gel techniques, microemulsion systems were formed by cetyl trimethyl ammonium bromide (CTAB) and 1-butanol in n-octane. The microemulsion containing an aqueous solution of $Fe(NO_3)_3$ and $Ga(NO_3)_3$ was mixed with another microemulsion containing NH_3 aqueous solution while rapidly stirring. Then tetraethoxysilane was added into the solution. This mixture was stirred for 20 hours and the materials were subsequently sintered at 1100 °C for 4 hours in air. The SiO_2 matrices were etched by a NaOH solution for 24 hours at 60 °C.

2.2 Morphology and crystal structure

In the transmission electron microscope (TEM) image, sphere-type particles with an average particle size between 20-40 nm are observed as shown in the inset of Figure 2. Rietveld analyses of X-ray diffraction (XRD) patterns indicate that materials of this series have an orthorhombic crystal structure in the $Pna2_1$ space group (Figure 3). This crystal structure has four nonequivalent Fe sites (A-D), i.e., the coordination geometries of the A-C sites are octahedral [FeO_6] and that of the D site is tetrahedral [FeO_4]. For example, in the case of x= 0.61, 92% of the D sites and 20% of the C sites are substituted by Ga^{3+} ions, but the A and B sites are not substituted because Ga^{3+} (0.620 Å), which has a smaller ionic radius than Fe^{3+} (0.645 Å),[22] prefers the tetrahedral sites. The shade of blue in Figure 3 depicts the degree of Ga substitution.

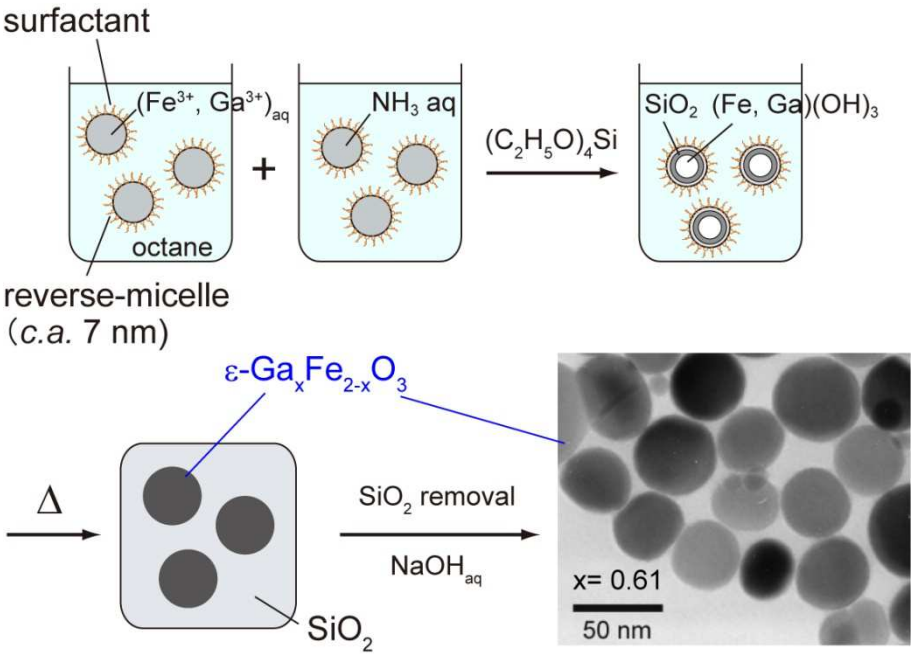

Fig. 2. Schematic illustration of the synthetic procedure of ε-$Ga_xFe_{2-x}O_3$ nanocrystal using combination method between reverse-micelle and sol-gel techniques. The inset is TEM image of ε-$Ga_xFe_{2-x}O_3$ particles.

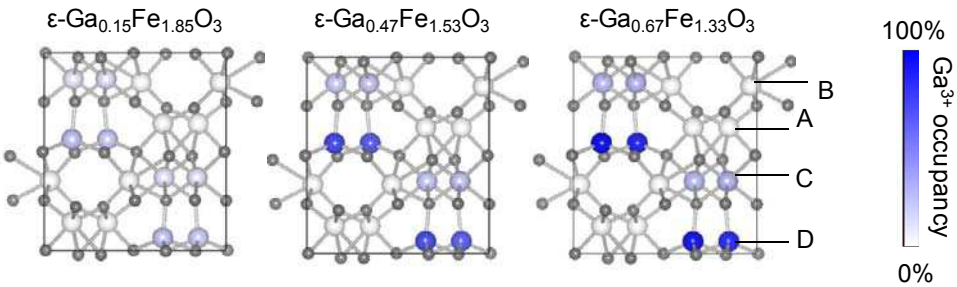

Fig. 3. Crystal structure of ε-$Ga_xFe_{2-x}O_3$. Degrees of Ga substitution at each Fe site (A–D) described by the shade of blue.

2.3 Magnetic properties

The magnetic properties of this series are listed in Table 1. The field-cooled magnetization curves in an external magnetic field of 10 Oe show that the T_C value monotonously decreases from 492 K (x= 0.10) to 324 K (x= 0.67) as x increases (Figure 4a). Figure 4b shows the magnetization vs. external magnetic field plots at 300 K. The H_c value decreases from 15.9 kOe (x= 0.10) to 2.1 kOe (x= 0.67). The saturation magnetization (M_s) value at 90 kOe increases from 14.9 emu g^{-1} (x= 0.10) to 30.1 (x= 0.40) and then decreases to 17.0 (x= 0.67).

		x= 0.10	x= 0.22	x= 0.29	x= 0.35	x= 0.40	x= 0.47	x= 0.54	x= 0.61	x= 0.67
T_C (K)		492	470	453	441	432	407	385	355	324
M_s (emu/g)	300 K	14.9	24.7	27.4	28.7	30.1	28.5	25.4	23.3	17.0
	2 K	19.2	36.1	42.1	47.5	52.0	52.7	51.0	51.6	42.8
H_c (kOe)	300 K	15.9	11.6	10.0	9.3	8.8	6.8	5.5	4.7	2.1
	2 K	15.5	15.7	14.1	13.7	13.4	12.8	13.1	13.7	14.2

Table 1. Magnetic properties of ε-$Ga_xFe_{2-x}O_3$.

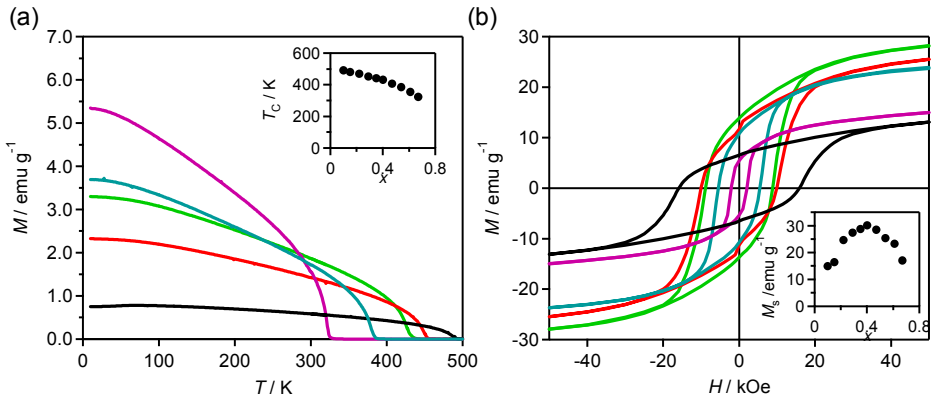

Fig. 4. Magnetic properties of ε-$Ga_xFe_{2-x}O_3$. (a) FCM curves for x= 0.10 (black), 0.22 (red), 0.40 (green), 0.54 (light blue), and 0.67 (magenta) in the external magnetic field of 10 Oe. (b) Magnetization vs. external field plots for x= 0.10 (black), 0.22 (red), 0.40 (green), 0.54 (light blue), and 0.67 (magenta).

The changes in magnetic properties were understood by the replacement of magnetic Fe^{3+} (S= 5/2) by non-magnetic Ga^{3+} ($3d^{10}$, S= 0). ε-Fe_2O_3 is a collinear ferrimagnet at room temperature where the magnetic moments at the B and C sites (M_B and M_C sublattice magnetization) are antiparallel to the A and D sites (M_A and M_D sublattice magnetization), i.e., $M_{total} = M_B + M_C - M_A - M_D$.[15,23] In addition, M_D sublattice magnetization is smaller than the other three sublattice magnetization. Ga^{3+} substitution reduces the M_D sublattice magnetization value due to selective substitution at the D sites in the region of $0.10 \leq x \leq 0.40$. Hence, M_{total} values of ε-$Ga_xFe_{2-x}O_3$ system increase as the x values increase. On the other hand, the decrease of M_{total} at $0.47 \leq x$ is caused by Ga replacement at the C, B, and A sites.

3. Millimeter wave absorption of ε-$Ga_xFe_{2-x}O_3$ nanomagnets

In this section, we deal with the millimeter wave absorption due to the natural resonance in ε-$Ga_xFe_{2-x}O_3$ nanoparticles.

3.1 Natural resonance

In general, when an EM wave is irradiated into a ferromagnet, the gyromagnetic effect leads to resonance, which is called a "natural resonance" (Figure 5a). In a ferromagnetic material

with a magnetic anisotropy, the direction of magnetization is restricted around the magnetic easy-axis. Once an external magnetic field tilts the magnetization, then the magnetization starts to precesses around the easy-axis due to the gyromagnetic effect. When this precession of magnetization resonates with an applied EM wave, a natural resonance occurs and EM wave absorption is observed.[24] The natural resonance frequency (f_r) is proportional to the magnetocrystalline anisotropy (H_a), which is expressed by $f_r = (\nu/2\pi)H_a$, where ν is the gyromagnetic ratio. Common magnetic materials such as spinel ferrite show EM wave absorption in a few GHz region, and even a f_r value of metal-substituted barium ferrite is 80 GHz or less.

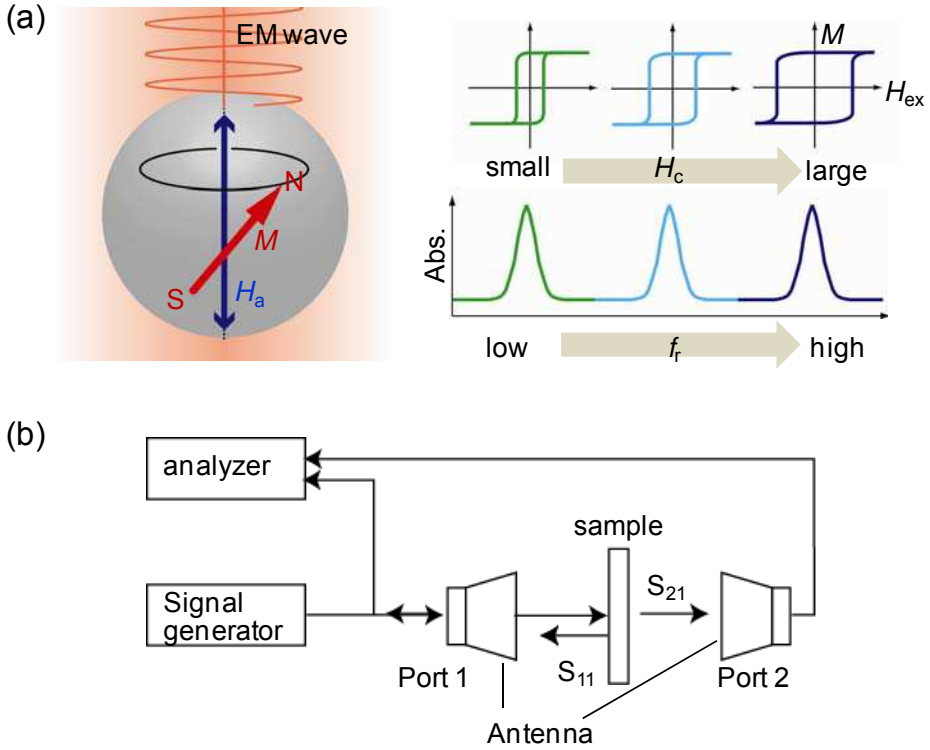

Fig. 5. (a) Schematic illustration of the natural resonance due to the gyromagnetic effect. Precession of magnetization (M) around an anisotropy field (H_a) causes electromagnetic wave absorption. Resonance frequency (f_r) is expressed as $f_r = (\nu/2\pi)\, H_a$. In magnets of a uniaxial magnetic anisotropy, f_r is proportional to magnetic coercive field (H_c). (b) Diagram of the free space millimeter wave absorption measurement system.

3.2 Millimeter wave absorption properties

The EM absorption properties (V-band; 50-75 GHz, and W-band; 75–110 GHz) were measured at room temperature using a free space EM wave absorption measurement system (Figure 5b). The powder-form samples were filled in a 30 mmϕ × 10 mm quartz cell with the fill ratios of *ca.* 40%. The reflection coefficient (S_{11}) and permeability coefficient (S_{21}) were

obtained, and the absorption of the EM waves was calculated by the following equation: (Absorption) = -10log[$|S_{21}|^2/(1-|S_{11}|^2)$] (dB). An absorption of 20 dB indicates that 99% of the introduced EM waves are absorbed, which is the target value for EM absorbers from an industrial point of view.

The center of Figure 6 shows millimeter wave absorption spectra of the samples between x= 0.61 and 0.29 in the frequency region of 50–110 GHz. The sample for x= 0.61 shows a strong absorption at 54 GHz. As x decreases, the frequency of the absorption peak shifts to a higher one, i.e., 64 GHz (x= 0.54), 73 GHz (x= 0.47), 84 GHz (x= 0.40), 88 GHz (x= 0.35), and 97 GHz (x= 0.29). In the case of samples for x= 0.67, 0.22, 0.15 and 0.10, the absorption peaks exceed the measurement range (50–110 GHz). To confirm the frequency of these materials, hand-made apparatuses for the range of 27–40 GHz and 105–142 GHz were prepared. As a result, the sample for x= 0.67 showed the absorption peak at 35 GHz (Figure 6, left). In the frequency range of 105–142 GHz, the peak frequencies for x= 0.22 and 0.15 are observed at 115 and 126 GHz, respectively, and that for x= 0.10 is estimated to be observed at 147 GHz by supplementation of the spectrum using the Lorentzian function (Figure 6, right). The absorption intensities of this series are strong (for example, the absorption intensity for x= 0.40 reaches 57 dB (99.9998%)).

As mentioned above, the f_r value is proportional to the magnetocrystalline anisotropy field (H_a), which is expressed by $f_r = (\nu/2\pi)H_a$ where ν is the gyromagnetic ratio. When the sample consists of randomly oriented magnetic particles with a uniaxial magnetic anisotropy, the H_a value is proportional to the H_c value. Figure 7 shows the relationship between f_r and the H_c values in the present series.

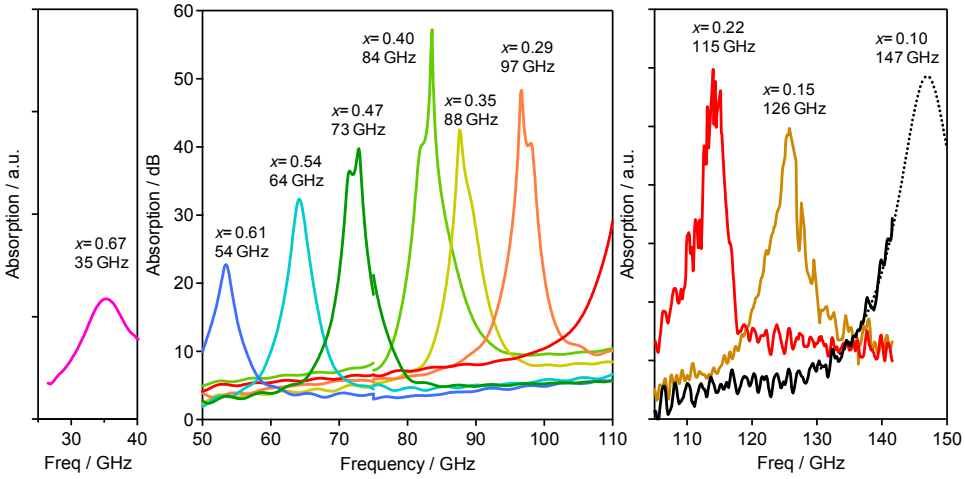

Fig. 6. Millimeter wave absorption properties of ε-$Ga_xFe_{2-x}O_3$. (left) Millimeter wave absorption spectra for x= 0.67 (gray) in the range of 27–40 GHz. (center) Millimeter wave absorption spectra for x= 0.61 (blue), 0.54 (light blue), 0.47 (green), 0.40 (light green), 0.35 (yellow), 0.29 (orange), and 0.22 (red) in the range of 50–110 GHz. (right) Millimeter wave absorption spectra for x= 0.22 (red), 0.15 (ocher) and 0.10 (black) using a hand-made apparatus in the range of 105–142 GHz. The peak of the spectrum for x= 0.10 is supplemented by the line fitted by the Lorentzian function (dotted black line).

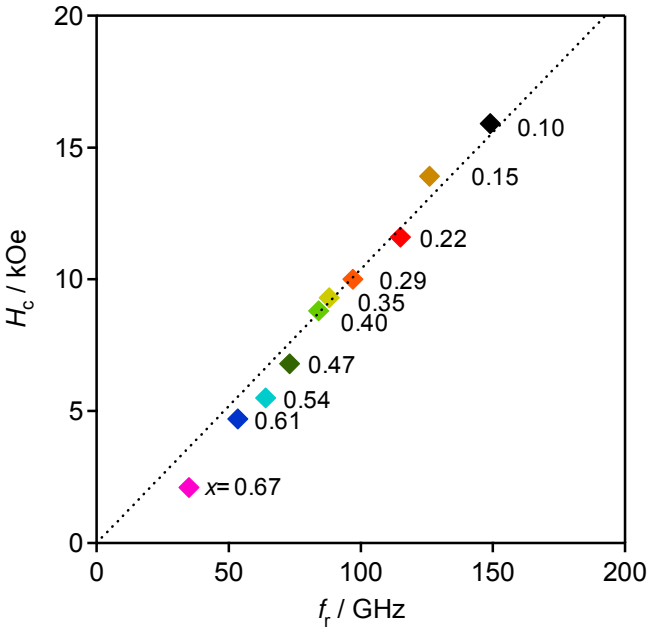

Fig. 7. Relationship between f_r and H_c of ε-$Ga_xFe_{2-x}O_3$.

4. Magnetic permeability (*μ*) and dielectric constant (*ε*) of ε-$Ga_xFe_{2-x}O_3$ nanomagnets

The metal substituted ε-Fe_2O_3 has attracted much attention as a potential stable EMI suppression material for millimeter wave electronics such as isolators and circulators.[20,25] The magnetic permeability of such millimeter wave absorbers is important to determine the attenuation and reflection properties, for the purpose of designing a millimeter wave absorber painted on a wall. Here we describe the reflectance and transmittance data of a series of ε-$Ga_xFe_{2-x}O_3$ (x= 0.51, 0.56, 0.61) in the region of 60 GHz band (V-band) and the evaluation of the magnetic permeability.

4.1 Theoretical background – Magnetic permeability near the natural resonance

The motion of magnetization can be described by the Landau-Lifshitz equations as follows:[26,27]

$$\frac{d\boldsymbol{M}}{dt} = -\nu\left(\boldsymbol{M}\times\boldsymbol{H}\right) - \frac{4\pi\mu_0\lambda}{M^2}\left(\boldsymbol{M}\times\left(\boldsymbol{M}\times\boldsymbol{H}\right)\right), \tag{1}$$

where $\boldsymbol{M}$ is a vector of magnetization, $\boldsymbol{H}$ is a vector of magnetic field, μ_0 is the vacuum magnetic permeability, and ν is the gyromagnetic coefficient. The first term describes magnetization precessing toward the direction of -($\boldsymbol{M}$ × $\boldsymbol{H}$), whereas the second term is for the case where braking acts on the precession and magnetization receives force in the direction of ($\boldsymbol{M}$ × ($\boldsymbol{M}$ × $\boldsymbol{H}$)). λ is the coefficient called the relaxation frequency, which

represents the degree of braking with a unit of Hz. By solving Eq. (1), the magnetic permeability at frequency of f is obtained as:

$$\mu'(f) = \frac{\nu M^2}{4\pi\mu_0 \lambda H_a} \sin\varphi(f)\cos\varphi(f) + 1 , \tag{2}$$

$$\mu''(f) = \frac{\nu M^2}{4\pi\mu_0 \lambda H_a} \sin^2\varphi(f) , \tag{3}$$

where H_a is the anisotropy field and $\varphi(f)$ is described by:

$$\varphi(f) = \tan^{-1}\left(\frac{4\pi\mu_0\lambda}{\nu M} \frac{H_a}{H_a - 2\pi f/\nu} \right). \tag{4}$$

As shown in Figure 8, $\mu'(f)$ shows dispersive-shaped lines around the natural resonance frequency f_r, while $\mu''(f)$ shows absorption peaks at f_r, where f_r is described by $f_r = \nu H_a/2\pi$.

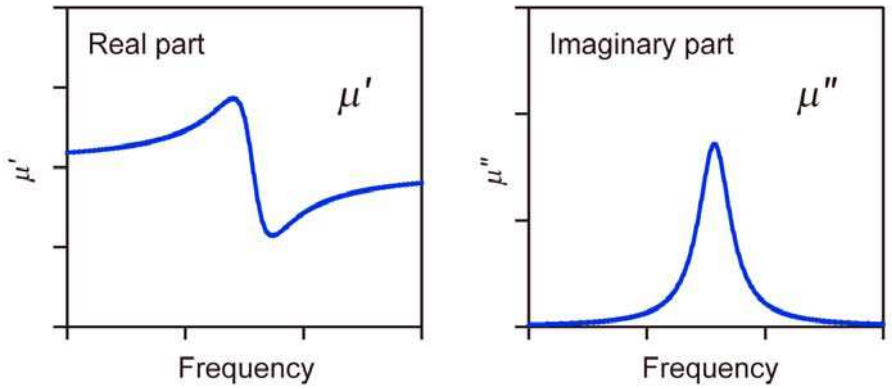

Fig. 8. Theoretical behavior of magnetic permeability around natural resonance.

4.2 Determination of magnetic permeability (μ) and dielectric constant (ε)

The reflectance (S_{11}) and transmittance (S_{21}) were measured by a free space EM wave absorption measurement system. Powder form samples were filled on a foam polystyrene holder with a 0.5 mm gap (filling ratio was *ca.* 20 vol. %). EM waves in the V-band (50-75 GHz) were irradiated vertically into the sample, and the transmitted and reflected waves were analyzed using waveguides and vector network analyzer. Figure 9a shows the measured S_{11} and S_{21} values in V-band. The absorption peaks of the transmitted waves were observed around 65 GHz (x= 0.51), 59 GHz (x= 0.56), and 55 GHz (x= 0.61). The reflected waves exhibited similar absorptions.

Using the measured S_{11} and S_{21} values, the magnetic permeability and dielectric constant were determined via the following procedure. When EM waves are irradiated vertically into a material, the reflection coefficient (Γ) and transmission coefficient (T) are represented as follows:

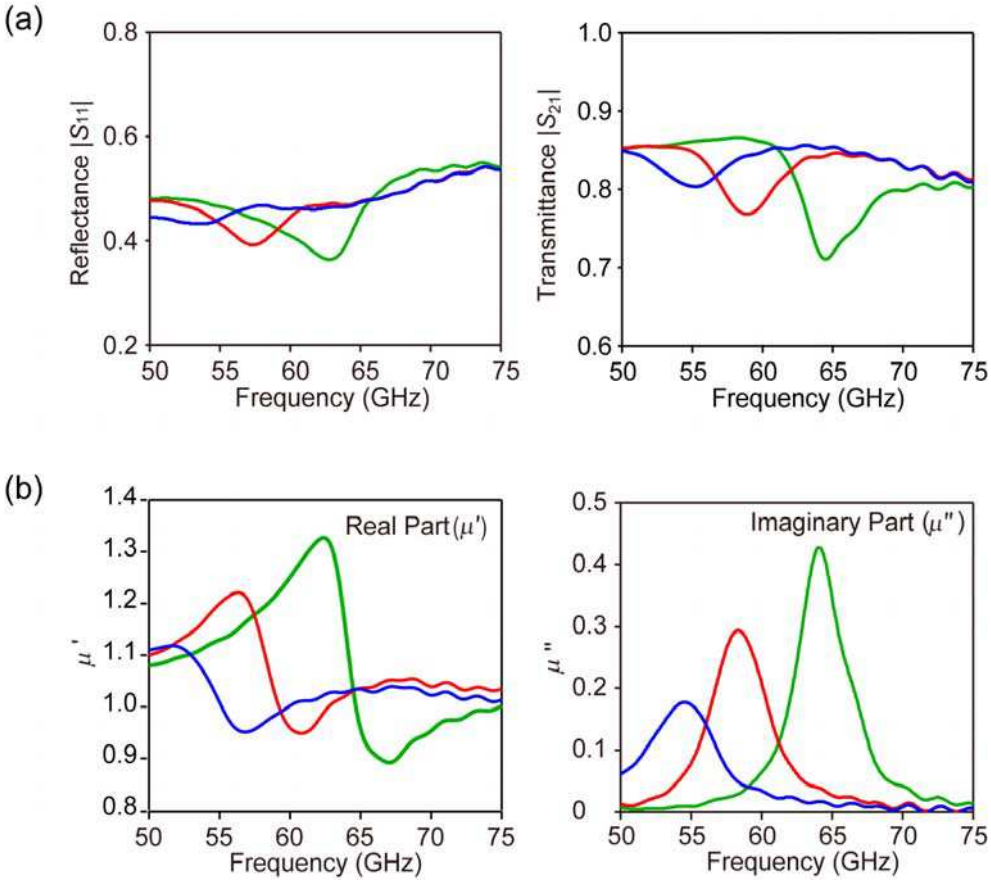

Fig. 9. (a) Reflectance and transmittance of ε-$Ga_xFe_{2-x}O_3$ for x= 0.51 (green), 0.56 (red), and 0.61 (blue). (b) the magnetic permeability of ε-$Ga_xFe_{2-x}O_3$ for x= 0.51 (green), 0.56 (red), and 0.61 (blue).

$$\Gamma = \frac{\sqrt{\mu_r/\varepsilon_r} - 1}{\sqrt{\mu_r/\varepsilon_r} + 1}, \tag{5}$$

$$\mathrm{T} = \exp\left(-jd\omega\sqrt{\varepsilon_0\varepsilon_\mathrm{r}\mu_0\mu_\mathrm{r}}\right), \tag{6}$$

where μ_0 is the vacuum magnetic permeability, ε_0 is the vacuum dielectric constant, μ_r is the relative magnetic permeability of the materials, ε_r is the relative dielectric constant, d is the thickness of the material, and j is the imaginary unit. Considering the effect of multiple reflections using the Nicolson-Ross Weir model,[28,29] the reflectance (S_{11}) and transmission (S_{21}) are represented by Γ and T as follows:

$$\mathrm{S}_{11} = \frac{\Gamma\left(1 - T^2\right)}{1 - \Gamma^2 T^2}, \tag{7}$$

$$\mathrm{S}_{21} = \frac{\left(1 - \Gamma^2\right)T}{1 - \Gamma^2 T^2}, \tag{8}$$

Using Eqs. (5)–(8), ε_r and μ_r of ε-$Ga_xFe_{2-x}O_3$ (x= 0.51, 0.56, 0.61) were determined from the measured S_{11} and S_{21} values. Figure 9b shows the determined magnetic permeability and dielectric constant of ε-$Ga_xFe_{2-x}O_3$. The μ'' values reached a maximum around 60 GHz; $\mu''_{\max}$= 0.43 (64 GHz), $\mu''_{\max}$= 0.29 (58 GHz), and $\mu''_{\max}$= 0.18 (55 GHz) for x= 0.51, 0.56, and 0.61, respectively. On the other hand, the real part of magnetic permeability showed dispersive-shaped lines at 65 GHz (x= 0.51), 59 GHz (x= 0.56), and 54 GHz (x= 0.61). Regarding dielectric constant, all samples did not show any significant variation. The sample for x= 0.51 exhibited $\mu''_{\max}$ of 0.43 at 64 GHz, which is the highest $\mu''_{\max}$ value among reported millimeter wave absorber in V-band region.[30]

5. Summary and prospective

In this article, we reported a millimeter wave absorber composed of ε-$Ga_xFe_{2-x}O_3$. This absorber can absorb millimeter waves in a wide range between 35–147 GHz. In addition, the μ'' values of ε-$Ga_xFe_{2-x}O_3$ are the highest values among reported magnetic millimeter wave absorbers in the V-band region, which means this series of materials can absorb millimeter waves with high efficiency. These new materials will be suitable for an absorber to restrain the EMI (for example, a millimeter wave absorber painted on the wall of office, private and medical room, or the body of car, train, and airplane), and an optoelectronic device to stabilize the EM sending (for example, a circulator and an isolator for millimeter waves of needless magnetic field).

6. References

[1] C. H. Doan, S. Emami, A. M. Niknejad and R. W. Brodersen, IEEE J. Solid-State Circuits 40, 144 (2005).

[2] M. J. W. Rodwell, *High Speed Integrated Circuit Technology, towards 100 GHz Logic* (World Scientific, Singapore, 2001).
[3] C. Cao, E. Seok and K. K. O, IEE Electronics Lett. 42, 208 (2006).
[4] B. R. Wu, W. Snodgrass, M. Feng and K. Y. Cheng, J. Crystal Growth 301-302, 1005 (2007).
[5] W. Snodgrass, B. R. Wu, W. Hafez, K. Y. Cheng and M. Feng, Appl. Phys. Lett. 88, 222101.
[6] K. J. Vinoy and R. M. Jha, *Radar Absorbing* (Kluwer, Boston, 1996).
[7] A. Vilcot, B. Cabon and J. Chazelas, *Microwave Photonics* (Kluwer, Boston, 1996).
[8] Y. Naito and K. Suetake, IEEE Trans. Microwave Theory Tech. 19, 65 (1971).
[9] Committee on identification of research needs relating to potential biological or adverse health effects of wireless communications devices, National Research Council *Identification of Research Needs Relating to Potential Biological or Adverse Health Effects of Wireless Communication* (National Academies Press, Washington, 2008).
[10] J. Jin, S. Ohkoshi and K. Hashimoto, Adv. Mater. 16, 48 (2004).
[11] S. Ohkoshi, S. Sakurai, J. Jin and K. Hashimoto, J. Appl. Phys. 97, 10K312 (2005).
[12] S. Sakurai, J. Jin, K. Hashimoto and S. Ohkoshi, J. Phys. Soc. Jpn. 74, 1946 (2005).
[13] E. Tronc, C. Chanéac and J. P. Jolivet, J. Solid State Chem. 139, 93 (1998).
[14] E. Tronc, C. Chanéac and J. P. Jolivet, J. M. Grenèche, J. Appl. Phys. 98, 053901 (2005).
[15] M. Gich, C. Frontera, A. Roig, E. Taboada, E. Molins, H. R. Rechenberg, J. D. Ardisson, W. A. A. Macedo, C. Ritter, V. Hardy, J. Sort, V. Skumryev and J. Nogues, Chem. Mater. 18, 3889 (2006).
[16] M. Popovici, M. Gich, D. Niznansky, A. Roig, C. Savii, L. Casas, E. Molins, K. Zaveta, C. Emache, J. Sort, S. Brion, G. Chouteau and J. Nogues, Chem. Mater. 16, 5542 (2004).
[17] M. Kurmoo, J. Rehspringer, A. Hutlova, C. D'Orleans, S. Vilminot, C. Estournes and D. Niznansky, Chem. Mater. 17, 1106 (2005).
[18] S. Sakurai, A. Namai, K. Hashimoto and S. Ohkoshi, J. Am. Chem. Soc., 131, 18299 (2009).
[19] S. Sakurai, K. Tomita, H.Yashiro, K. Hashimoto and S. Ohkoshi, J. Phys. Chem. C., 112, 20212 (2008).
[20] S. Ohkoshi, S. Kuroki, S. Sakurai, K. Matsumoto, K. Sato and S. Sasaki, Angew. Chem. Int. Ed. 46, 8392 (2007).
[21] A. Namai, S. Kurahashi, H. Hachiya, K. Tomita, S. Sakurai, K. Matsumoto, T. Goto and S. Ohkoshi, J. Appl. Phys., 107, 09A955 (2010).
[22] R. D. Shannon, Acta Cryst. A 32, 751 (1976).
[23] S. Ohkoshi, A. Namai and S. Sakurai, J. Phys. Chem. C 113, 11235 (2009).
[24] S. Chikazumi, *Physics of Ferromagnetism* (Oxford University Press, New York, 1997).
[25] A. Namai, S. Sakurai, M. Nakajima, T. Suemoto, K. Matsumoto, M. Goto, S. Sasaki and S. Ohkoshi J. Am. Chem. Soc. 131, 1170 (2009).
[26] L. Landau and E. Lifshitz, Phys. Z. Sowjet-union 8, 153 (1935).
[27] A. Herpin, *Théorie du Magnétism* (Presses Universitaires de France, Paris, 1968).

[28] A. M. Nicolson and G. F. Ross, IEEE Transactions on instrumentation and measurement 19, 377 (1970).
[29] W. B. Weir, Proceedings of the IEEE, 62, 33 (1974).
[30] K. A. Korolev, L. Subramanian and M. N. Afsar, J. Appl. Phys. 99, 08F504 (2006).

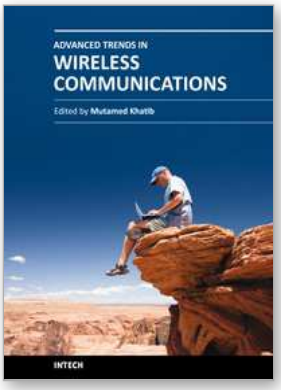

Advanced Trends in Wireless Communications

Edited by Dr. Mutamed Khatib

ISBN 978-953-307-183-1
Hard cover, 520 pages
Publisher InTech
Published online 17, February, 2011
Published in print edition February, 2011

Physical limitations on wireless communication channels impose huge challenges to reliable communication. Bandwidth limitations, propagation loss, noise and interference make the wireless channel a narrow pipe that does not readily accommodate rapid flow of data. Thus, researches aim to design systems that are suitable to operate in such channels, in order to have high performance quality of service. Also, the mobility of the communication systems requires further investigations to reduce the complexity and the power consumption of the receiver. This book aims to provide highlights of the current research in the field of wireless communications. The subjects discussed are very valuable to communication researchers rather than researchers in the wireless related areas. The book chapters cover a wide range of wireless communication topics.

How to reference

In order to correctly reference this scholarly work, feel free to copy and paste the following:

Asuka Namai and Shin-ichi Ohkoshi (2011). High-frequency Millimeter Wave Absorber Composed of a New Series of Iron Oxide Nanomagnets, Advanced Trends in Wireless Communications, Dr. Mutamed Khatib (Ed.), ISBN: 978-953-307-183-1, InTech, Available from: http://www.intechopen.com/books/advanced-trends-in-wireless-communications/high-frequency-millimeter-wave-absorber-composed-of-a-new-series-of-iron-oxide-nanomagnets

INTECH
open science | open minds

InTech Europe
University Campus STeP Ri
Slavka Krautzeka 83/A
51000 Rijeka, Croatia
Phone: +385 (51) 770 447
Fax: +385 (51) 686 166
www.intechopen.com

InTech China
Unit 405, Office Block, Hotel Equatorial Shanghai
No.65, Yan An Road (West), Shanghai, 200040, China
中国上海市延安西路65号上海国际贵都大饭店办公楼405单元
Phone: +86-21-62489820
Fax: +86-21-62489821